ORNL/TM-2021/2177

Demonstration of Dimensional and Microstructural Postirradiation Examination Capabilities on MiniFuel Disk Specimens

C.P. Massey
R.L. Seibert
A.G. Le Coq
J.M. Harp

July 2021

OAK RIDGE National Laboratory

ORNL IS MANAGED BY UT-BATTELLE LLC FOR THE US DEPARTMENT OF ENERGY

ORNL/TM-2021/2177

DOE National Nuclear Security Administration
Office of Defense Nuclear Nonproliferation and Office of Material Management

DEMONSTRATION OF DIMENSIONAL AND MICROSTRUCTURAL POST-IRRADIATION EXAMINATION CAPABILITIES ON MINIFUEL DISK SPECIMENS

C.P. Massey
R.L. Seibert
A.G. Le Coq
J.M. Harp

July 2021

Prepared by
OAK RIDGE NATIONAL LABORATORY
Oak Ridge, TN 37831-6283
managed by
UT-BATTELLE LLC
for the
US DEPARTMENT OF ENERGY
under contract DE-AC05-00OR227

CONTENTS

LIST OF FIGURES

ABBREVIATIONS

EBSD	electron backscatter diffraction
EDS	x-ray spectroscopy
FIB	focused ion beam
HEU	high-enriched uranium
LEU	low-enriched uranium
MiniFuel	miniature fuel
ORNL	Oak Ridge National Laboratory
PIE	postirradiation examination
SEM	scanning electron microscope

ACKNOWLEDGMENT

This work was supported by the US Department of Energy's National Nuclear Security Administration, Office of Defense Nuclear Nonproliferation and Office of Material Management and Minimization ^{99}Mo Program. Lastly, the authors thank Becky Johnson and Christopher Hobbs for RCT and sample preparation support, respectively.

ABSTRACT

This work demonstrates two new MiniFuel postirradiation examination (PIE) capabilities, laser profilometry and serial sectioning, for future use on alpha-U specimens for the upcoming Mini-99 irradiation campaign. Representative U–Mo disk specimens—3 mm in diameter and approximately 0.75 mm in thickness—were subjected to dimensional measurements using standard calipers, as well as a new Keyence CL-3000 series laser profilometry system designed to measure the surface of both sides of the disk simultaneously. The laser profilometry system captured thickness gradients across the specimens as large as 0.2 mm. Additionally, because of the limitations inherent to the use of calipers, caliper measurements consistently overestimated the initial volume of MiniFuel disk specimens compared to the laser profilometry method by up to 5%. However, the results show that optimal data collection and analysis procedures are crucial to avoiding significant artifacts during data collection that can lead to large errors (approximately 10%). Serial sectioning using a combination of ion milling and electron imaging was also demonstrated for the analysis of micron-sized control volumes. Nanometer- to micron-scale porosity was resolved on a representative U–Mo specimen before irradiation, even when the surface of the specimen appeared free of porosity. Future efforts to relate microstructural features (porosity, fission product distributions, and so on) to macroscale effects (dimensional changes, thermal conductivity degradation) require accurate characterization methods such as those demonstrated in this work. These advanced PIE capabilities will be applied to optimized alpha-U specimens for the upcoming Mini-99 neutron irradiation campaign.

1. INTRODUCTION

The Tc-99m isotope is used in 80% of all medical diagnostic imaging, but only a select few international research reactors supply ^{99}Mo for this purpose. Because demands on ^{99}Mo are projected to increase to supply ^{99m}Tc for medical applications, much effort has been focused on expanding the current production capacity of ^{99}Mo using conventional and advanced methodologies. The fission-produced ^{99}Mo isotope, with a half-life of 66 hours, beta decays into ^{99m}Tc, which has a half-life of only 6 hours. Therefore, it is important to establish efficient methods to produce ^{99}Mo and isolate this valuable isotope through chemical extraction methods, maximizing the available ^{99m}Tc for use in medical diagnostics.

Until recently, the ^{99}Mo supply in the United States has been produced entirely by research reactors operated in other countries, such as the National Research Universal reactor in Canada and the Petten High Flux Reactor in the Netherlands. This has placed the United States in a position in which unexpected supply chain disruptions have significantly affected the availability and price of ^{99m}Tc. Additionally, because of increasing concerns about proliferation risks, it is desired that future ^{99}Mo production occur using low-enriched uranium (LEU) targets instead of highly enriched uranium (HEU) targets [1–4]. In response to these needs, a New Mexico–based startup, Eden Radiopharmaceuticals, is developing its own commercial capabilities for ^{99}Mo production in the United States to reduce the country's reliance on imported ^{99}Mo. Eden is interested in high-density LEU foil targets to achieve this goal.

To accelerate the qualification and licensing of Eden's high-density annular target design, Oak Ridge National Laboratory (ORNL) and the Y-12 National Security Complex are spearheading two irradiation campaigns using the High Flux Isotope Reactor. The first irradiation campaign focuses on the irradiation of miniature fuel (MiniFuel) disks of LEU to elucidate irradiation dose and temperature trends on both thermal conductivity and dimensional stability. A second irradiation will be performed on a prototypic macroscale LEU annular target, and subsequent postirradiation examination (PIE) activities will be informed by the preliminary MiniFuel results.

Eventual PIE activities on irradiated MiniFuel LEU disks will comprise (1) laser flash diffusivity measurements, (2) laser profilometry dimensional measurements, (3) serial sectioning and porosity analysis for cavities greater than 1 μm in size, and (4) analytical electron microscopy for nanoscale cavity identification and quantification. This report highlights ORNL's laser profilometry and serial sectioning capabilities for pre- and postirradiation characterization. For each technique, data collection, analysis, and interpretation are discussed, focusing on the resolution achievable with each technique. Laser flash diffusivity measurements are not discussed in this report and will be covered in a future report. Because of material availability and the similarity in specimen geometry, 18 unirradiated MiniFuel U–Mo alloy disks were analyzed using the laser profilometry system, and one disk was evaluated using the serial sectioning approach.

2. LASER PROFILOMETRY DIMENSIONAL MEASUREMENTS

2.1 SYSTEM SPECIFICATIONS

The laser flash profilometry measurement system procured for this effort combines a Keyence CL-3000 fiber-optic laser system with an MCM3001 PLS-XY mechanical stage developed by Thorlabs. The system is specifically designed for implementation in a glove box environment because all controllers and optical units can be located outside of a glovebox. The sensor heads are the only components in potential contamination areas. The initial laser profilometry design setup is shown in Figure 1.

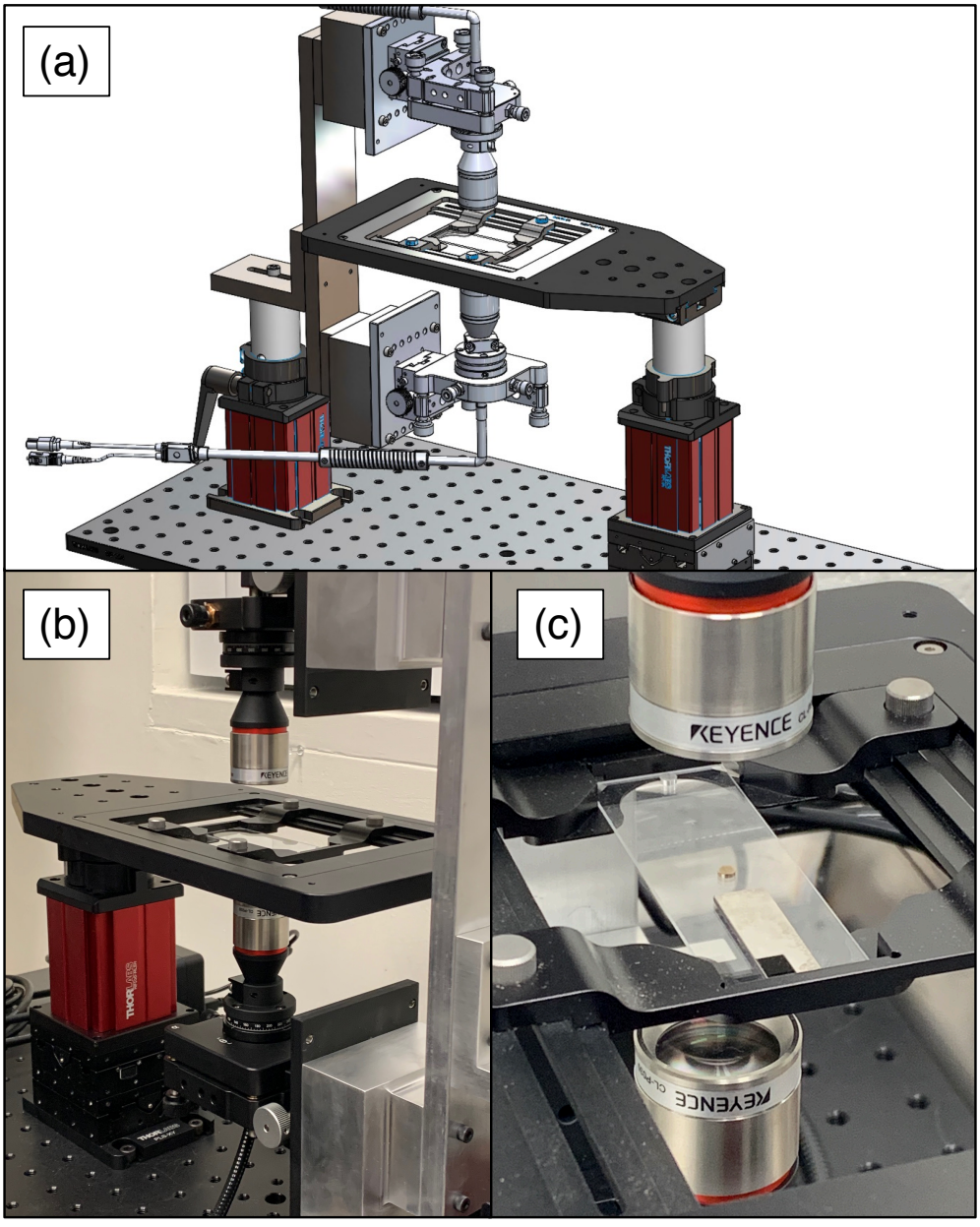

Figure 1. Keyence CL-3000/Thorlabs laser profilometry system. In (a) the initial SolidWorks rendition of the designed fixture is shown. In (b) the as-built setup is shown, whereas in (c) a smaller field-of-view highlights a miniature fuel geometry (3 mm disk) specimen centered on a glass slide during data collection.

The Keyence system uses two spot-type CL-P030 fiber-optic laser sensors to measure the thickness of a specimen, which is placed on a glass slide between the two sensor heads. The working distance of each sensor head is 30 ± 3.7 mm, allowing for thickness measurements of specimens as large as 1 cm in height. The CL-P030 sensors have a height precision of 0.94 µm and a spot size of 38 µm. Each sensor connects to a corresponding optical unit that outputs through a CL-3000 controller via USB to the support computer.

A custom support frame was machined to secure each stand at the correct distance to interface with a Keyence-supplied adjustable fixture for double–sensor head calibration (CL-P070). Sensor head alignment was performed in three stages. First, the horizontal and vertical incidence angles of each sensor head were adjusted to provide the highest reflected signal intensity, using the CL-P070 fixture shown in Figure 2a. Additionally, the reflective surface allowed for tuning the work offset to 30 mm, which is the desired working distance for both sensors. The second step consisted of coarse laser alignment by using a piece of paper as an opaque surface to visualize both laser spots (Figure 2b) and tuning the horizontal X/Y knobs so that the two spots overlapped. X and Y were finely adjusted by removing the fixture in Figure 2b and maximizing the measured signal intensity, which corresponds to the optimal alignment of the two sensor heads.

An MCM3000 series three-axis controller and a Thorlabs XY stage were used to mount an MP100 rigid stand with a built-in microscope slide holder. The XY stage has a 25 mm travel range with a 1 µm bidirectional repeatability. The minimum listed incremental movement is 100 nm, and the minimum listed repeatable incremental movement is 200 nm. Consequently, the less precise bidirectional repeatability results in an expected resolution of approximately 1 µm in the X and Y directions during data collection, even though the mechanical stage has a submicron movement capability.

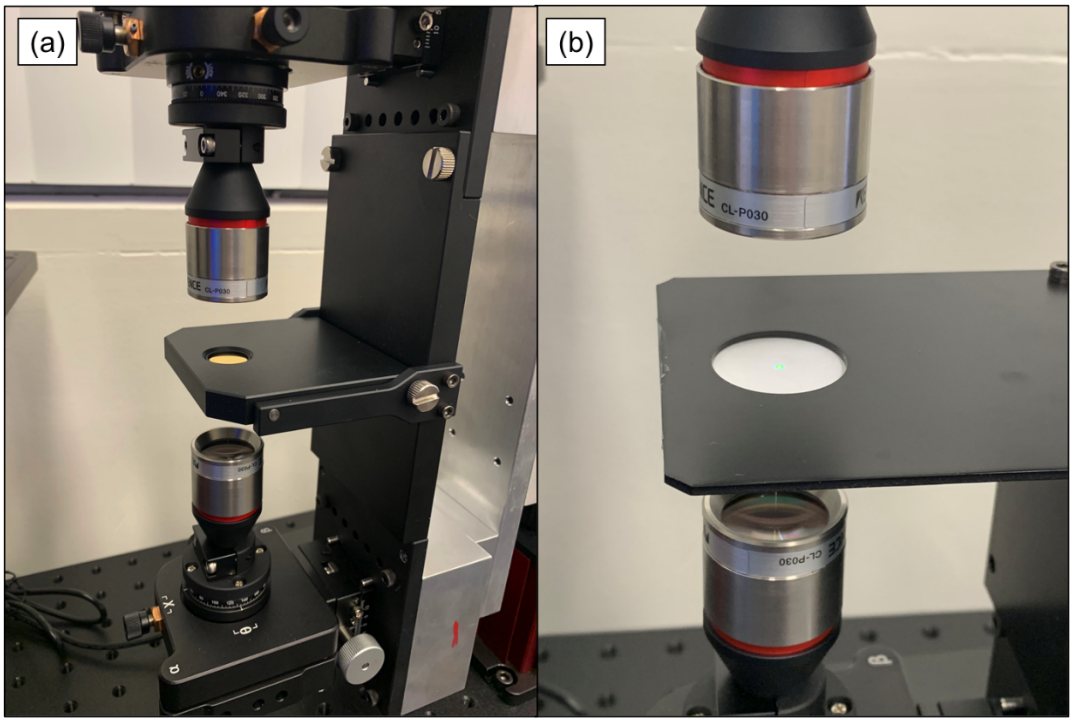

Figure 2. Fixture attachments used for sensor head alignment before laser profilometry data collection. In (a), a highly reflective surface is used to maximize the reflected laser intensity for both heads. In (b), coarse alignment is shown through a visual inspection of green laser spots through an opaque quite piece of paper.

The Keyence-supplied CL-NavigatorN software package was used for peak filtering and dimensional calibration. Peak filtering is needed for this specific application; the bottom sensor head requires the identification of two peak reflections because of the partial reflection of the glass slide sample support. Two conditions are presented in Figure 3, in which reflected intensities are either an empty glass slide or a slide with an additional specimen placed on top. In the first case, two relatively equal reflections are observed: the peak to the left corresponds to the first (nearer) reflection and the second (farther) peak corresponds to the second reflection. When a sample is placed on top, the second peak's intensity increases, whereas the first peak's intensity decreases. There are technically three associated reflections, but the second smaller reflection overlaps with a stronger reflection of the fully reflected peak that corresponds to the specimen on top of the glass slide. Occasionally, the existence of multiple peaks can cause confusion in the software's Boolean decision-making process. Since the bottom of the glass is a known constant distance from the bottom sensor head, this first peak is filtered out from the sensor's waveform.

Two Mitutoyo steel rectangular gauge blocks were used to calibrate the thickness measured by the two sensor heads. The two blocks, 0.5 mm and 1.16 mm, span the expected thickness range for the MiniFuel disks investigated here. Both calibration blocks are K-grade, with a dimensional deviation in the 200–300 nm range under standard temperature and pressure conditions. Thus, the two calibration blocks have a higher dimensional accuracy than the resolution of the sensors used in this work.

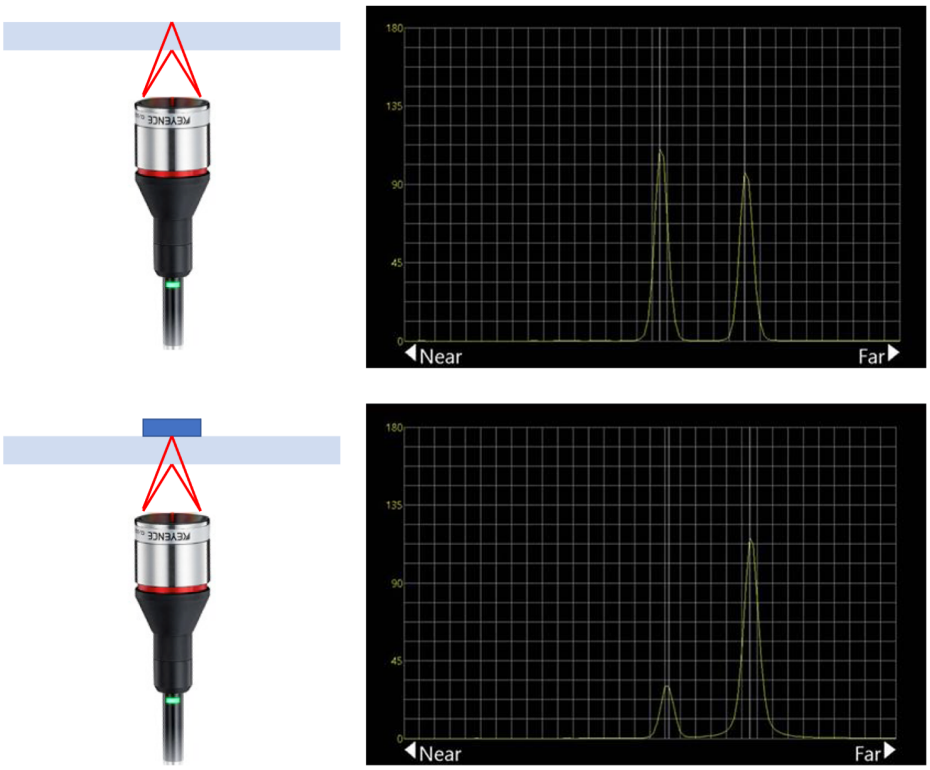

Figure 3. Reflected peak intensities (*top*) for conditions with reflections from the glass slide sample support only and (*bottom*) with an additional reflection from the specimen of interest.

2.2 DATA COLLECTION AND ANALYSIS

A custom LabVIEW program was developed to control the Thorlabs stage and collect the laser profilometry outputs. For the purposes of this work, the scan path of the laser followed a simple comb-raster pattern, allowing the laser to scan across all Y coordinates while held constant at each X value. A suitable scan area was chosen (3.5 mm × 3.5 mm) to ensure complete coverage for a 3 mm outer diameter MiniFuel disk specimen. The step size was 25 µm, which was chosen to achieve a balance between resolution and scan time.

The resulting output, exported to a comma-separated values (.csv) file, contains five columns: the two encoder values for the Thorlabs stage (X and Y), as well as OUT1 (bottom sensor displacement), OUT2 (top sensor displacement), and OUT3 (computed thickness). The raw thickness data are illustrated in Figure 4. The laser profilometry system (in the current scan configuration) provides a total of 19,600 dimensional measurement points, compared to the three single-caliper measurements that routinely occur for this type of work.

As with any type of measurement, the laser profilometry system contains some artifacts that are important to note. A close inspection of the data reveals that the thickness values are highly variable near the edges of the MiniFuel specimen, and nonphysical values are either negative or twice the actual thickness of the specimen. The negative thicknesses values (indicated by a dark blue/purple color on the left edge of the disk in Figure 4b) transition to positive values greater than the actual disk thickness as the scan progresses to the right edge of the same disk. This error is caused by a slight misalignment of the two laser heads during calibration, leading to instances in which the top laser remains off the sample of interest for 1–2 steps (25–50 µm) while the laser opposite to the top laser registers an actual disk surface measurement. Thus, this error can be minimized in the future through more detailed laser head calibration.

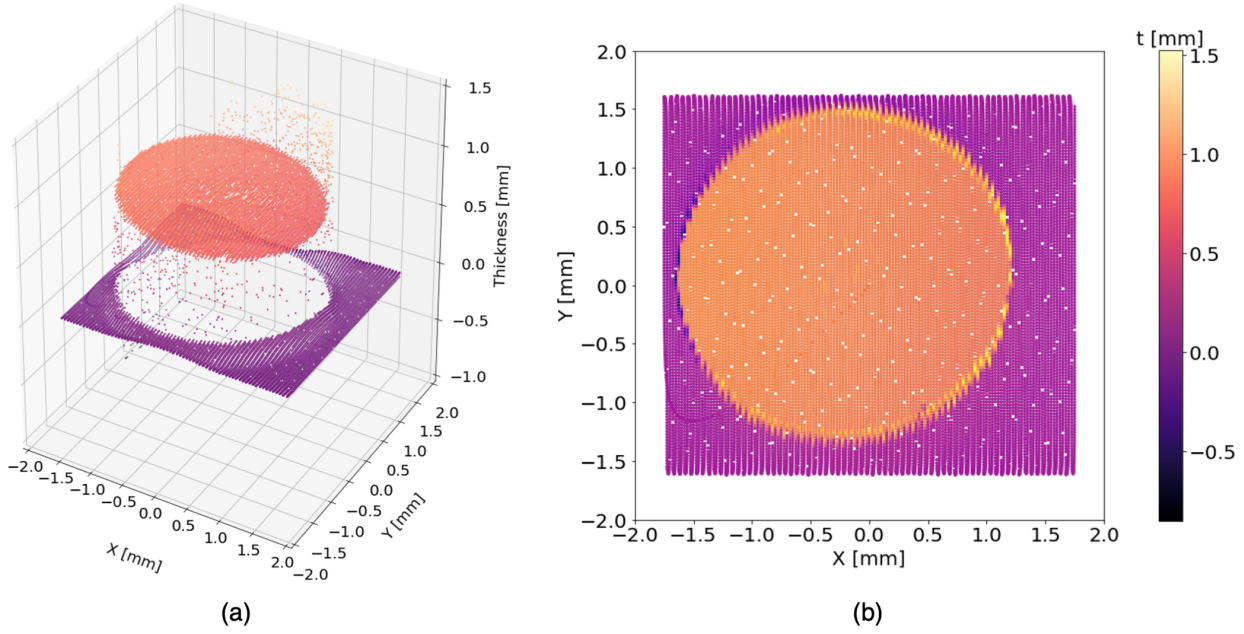

Figure 4. Example (a) 3D isometric view and (b) top view of raw dimensional data from a MiniFuel disk scan of U–Mo specimen 10Mo-2002-A. Points are colored as a function of measured material thickness.

The second artifact that is clearly noticeable in Figure 4 is an apparent saw-tooth morphology at the periphery of the disk. This discontinuity was found to be a function of scan path, scan speed, and data acquisition command timing. For example, consider the previous scan of a U–Mo disk shown in Figure 4,

which is replotted in Figure 5a with a smaller field of view. Using the same parameters, a surrogate 3 mm diameter, 1 mm thick Al disk was also scanned and is plotted in Figure 5b. This type of scan, for the purposes of this work, is called *continuous acquisition*: the stage movement command was sent to the Thorlabs stage, and data were immediately read from the Thorlabs and Keyence systems. Although the scan area supposedly ranged from −1.75 to 1.75 mm in both the X and Y orientations, the maximum Y dimension for both continuous acquisition scans only reached approximately 1.6 mm. Additionally, the saw-tooth perimeter is noted on both plots. These artifacts suggest that the XY stage was not reaching the desired setpoint before the unit received a new command for both data acquisition and follow-on movement.

Although the U–Mo disks in this report were analyzed in continuous acquisition mode, subsequent parametric optimization was performed to mitigate edge artifacts. Two time-delay options were tested in the LabVIEW program: a discrete delay and a full delay. In the discrete delay, a time period of 0.1 s elapsed between the XY stage movement command and the data acquisition command. This added delay greatly improved the data quality, as shown in Figure 5c. The other delay option is the full delay, which was modified so that the data acquisition command would not proceed until the error associated with the current stage position and the setpoint dropped below a threshold value. In a similar manner to the first delay option, the error further decreased and is plotted in Figure 5d. Additionally, both time delay options significantly decreased the variance in the point-to-point step size and in the thickness measured for the surrogate Al disk (Figure 6).

Unfortunately, both time delay options add significant analysis time to each disk scan. Whereas continuous acquisition requires only 7 min per disk, discrete delay increases scan time to 38 min, and full delay increases the scan time for each disk to 2.5 h. In practice, the discrete delay scan type may provide the best balance between scan time and dimensional accuracy because of accountable material handling requirements.

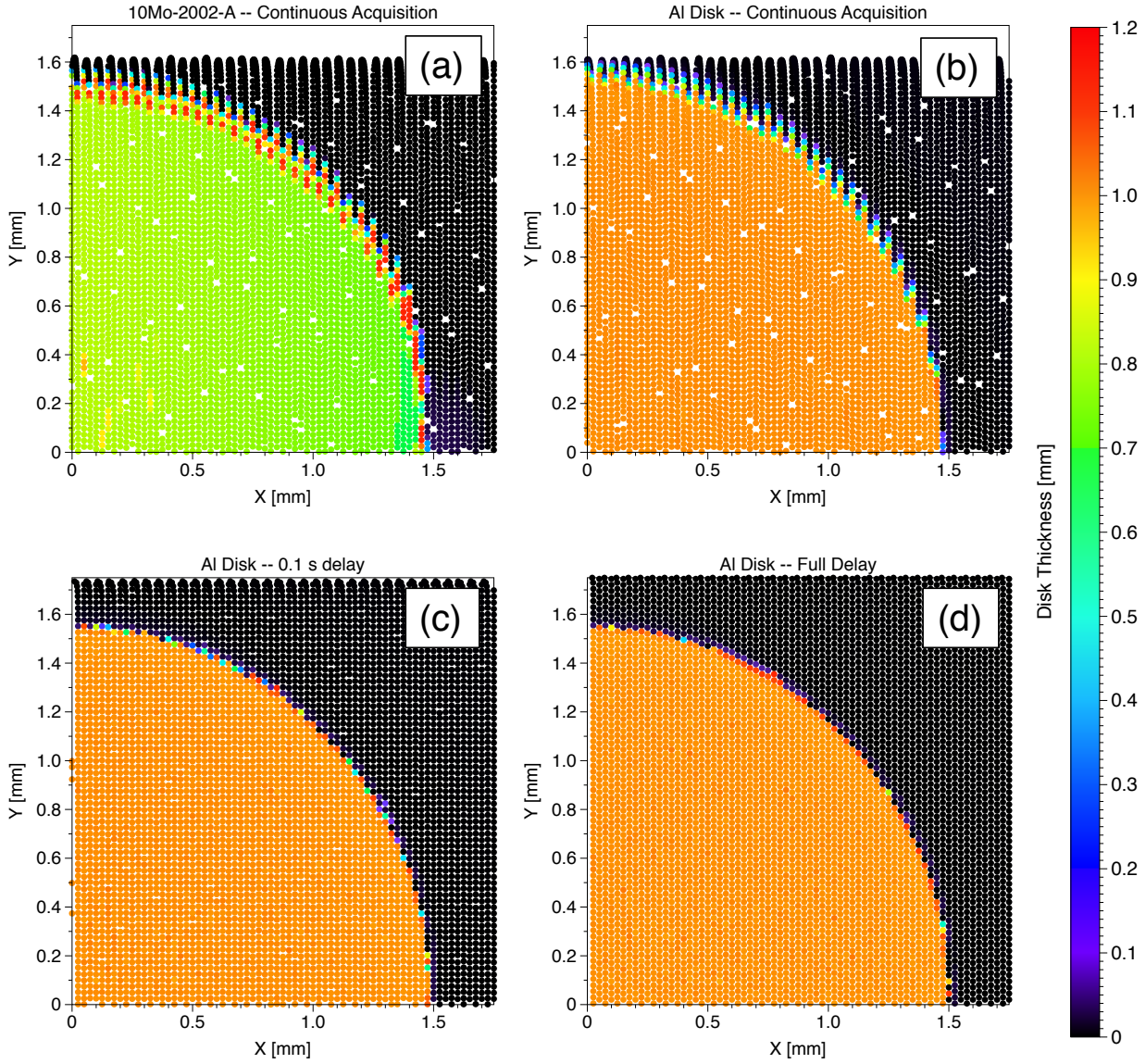

Figure 5. Scatterplots of disk thickness values for (a) U–Mo disk 10Mo-2002-A and (b–d) an Al disk of similar geometry. Continuous acquisition scan parameters were used in (a–b). In (c) a 0.1 s delay was implemented between travel and data acquisition, whereas in (d) a full delay was implemented.

After data acquisition, a Python script is used to filter the data, removing data points associated with the glass slide and outliers associated with edge effects. This combined DataFrame is converted into a volumetric rendering of the disk (Figure 8) by calculating an encapsulating surface using 3D Delaunay triangulation packages available in Python (Scipy). The following section includes a detailed discussion about this volume calculation methodology in comparison to conventional ones.

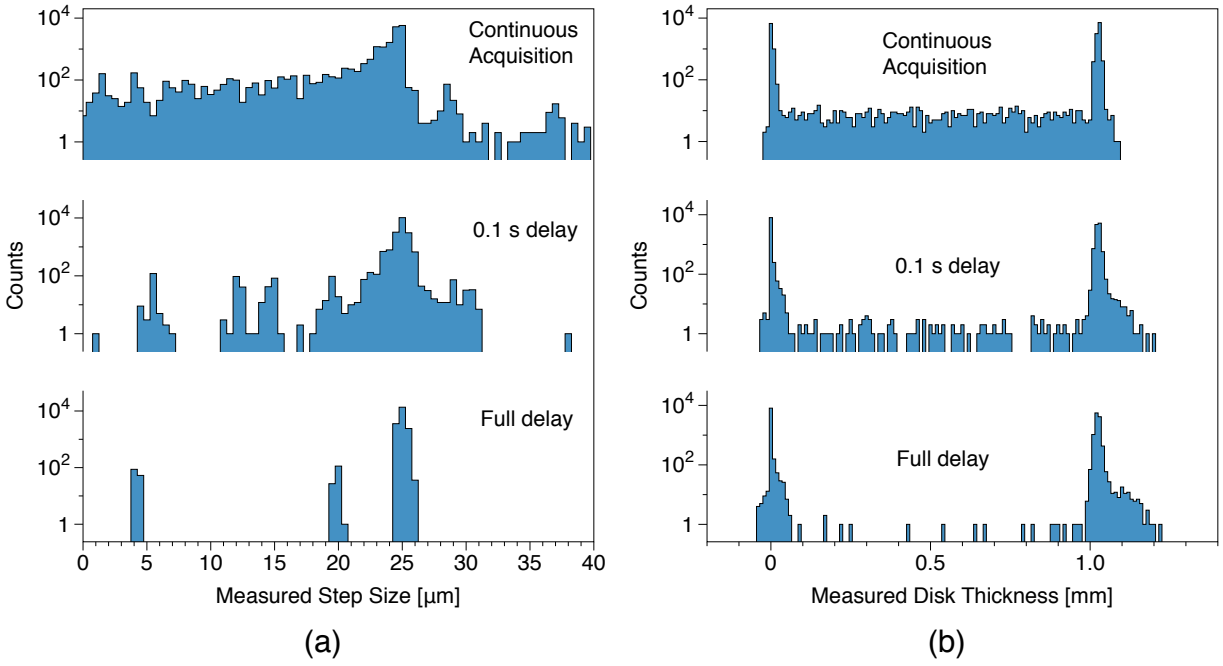

Figure 6. Histogram plots of (a) point-to-point step size and (b) measured disk thickness for a 1 mm thick Al disk used for parametric optimization.

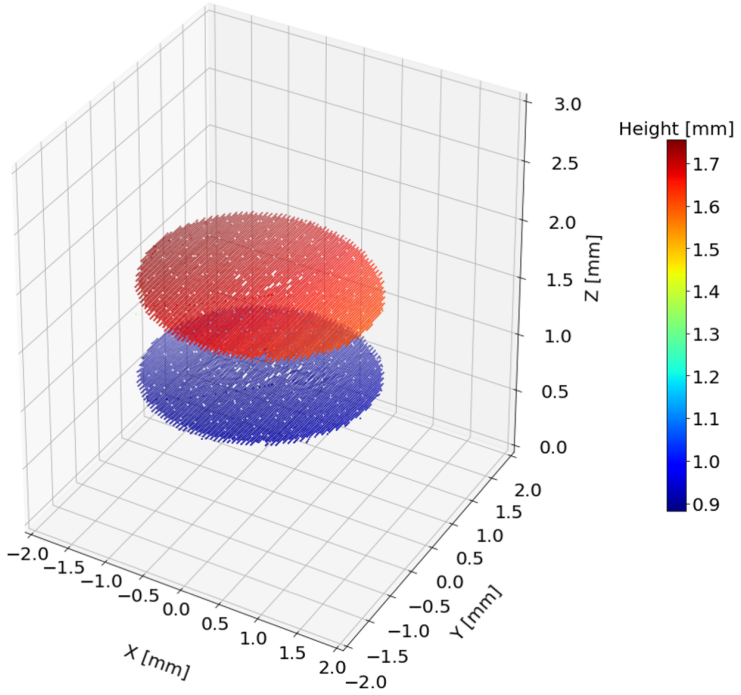

Figure 7. Filtered 3D isometric plot of the top and bottom surfaces of representative U–Mo disk specimen 10Mo-2002-A.

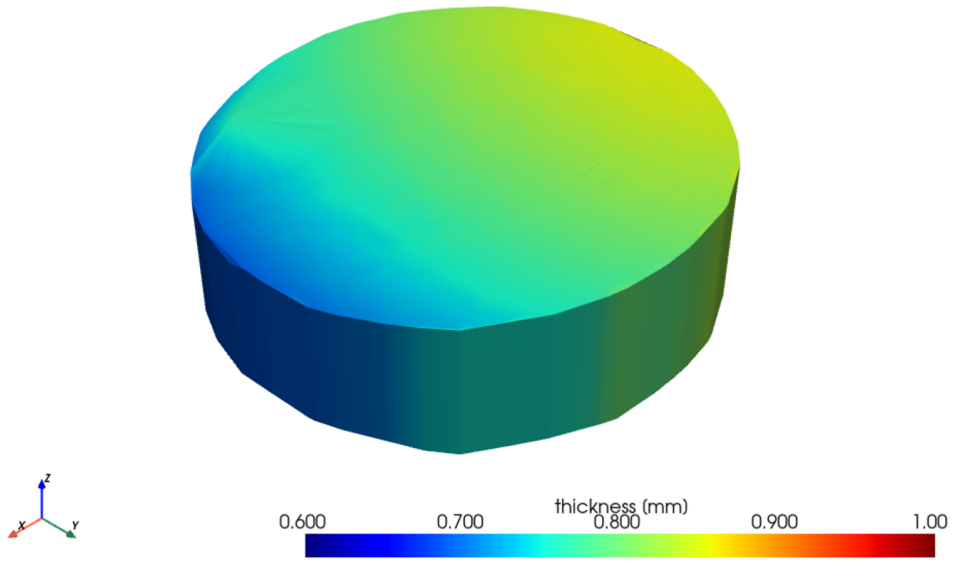

Figure 8. Volume rendering using the 3D Delaunay triangulation approach, colorized as a function of disk thickness for U–Mo disk specimen 10Mo-2002-A.

2.3 TECHNIQUE COMPARISONS

This section covers the differences in volume calculations for 18 U–Mo MiniFuel disk specimens compared to results estimated using standard caliper measurements. Although alpha-U disks will eventually be used for Eden's MiniFuel irradiation campaign, the U–Mo disks are of similar dimensions, and alpha-U material was not available at the time this report was prepared. Instead, these samples provide a proof-of-concept for the use of the Keyence CL-3000 series laser profilometry system for high-fidelity volumetric measurements. They will also provide insights to inform scan parameters used for the eventual evaluation of the alpha-U disks.

The 18 MiniFuel specimens presented here were analyzed using the continuous acquisition scan parameters. Consequently, all specimens show the same artifacts as the 10Mo-2002-A specimen. Aside from the edge effects discussed in the previous section, the laser profilometry method showed significant variations in thickness across individual specimens and between multiple specimens. As Figure 9 illustrates, many of the specimens analyzed show a gradient in specimen thickness across the sample width. This is an important insight that simple caliper measurements would not usually capture, since a caliper or micrometer tend to measure the largest thickness value based on degrees of freedom constraints. The laser profilometry system resolved thickness variations across individual specimens that exceed 200 µm. This is a small deviation, but because it measures total thickness averaging 700 µm, it is a considerable variation that could lead to erroneous postirradiation growth and/or swelling measurements.

The volume of each disk was calculated in four different ways, and the results are listed in Table 1. The first method used the point cloud of filtered dimensional data from the Keyence system to calculate the volume of the convex hull enclosing all the disk's datapoints. This volume is labeled "V_k (Convex Hull)" in the table. The other three volumes are based on the simple formula for cylindrical volume $V = \pi R^2 t$, where V is the volume, R is the radius, and t is the disk thickness. The radius and thickness values are tabulated either using thickness measured with calipers (R_c/t_c) or thickness measured with the filtered Keyence data (R_k/t_k). The three resulting volumes were computed using either only caliper values (R_c & t_c) or a mixture of caliper and Keyence values (R_c & t_k) and (R_k & t_k). The

combination of (R_k & t_c) was not computed because of the non-ideal nature of this combination, as is discussed below.

First and foremost, the use of the continuous acquisition approach leads to erroneous edge artifacts for each scan. As a result, there is a constant difference of approximately 80 μm in the average radius measured between the calipers and the Keyence method. Because of this underestimation of the specimen diameter using the non-optimized scan parameters of the Keyence system, the volumes computed via the convex hull method and any calculation using the Keyence radius (R_k) resulted in volumetric differences up to 10–15% compared to those calculated using only caliper measurements. It is expected that the use of discrete delay options in the scan methodologies will converge the measured radii between the two systems.

In lieu of additional discrete delay or full delay data for the presented U–Mo specimens, it is worthwhile to compare the volumes calculated using (1) caliper radius and (2) the average radii computed via both caliper and Keyence methods. The result, from an integrated volume standpoint, is a disk with area $A = \pi R_c^2$ extruded over a thickness equivalent to either the caliper-measured thickness (t_c) or the Keyence-measured thickness (t_k). The result is a scattered but monotonically increasing difference in computed volume of each analyzed disk that scales as a function of the variation of thickness across each disk. In all but one case in Table 1, the measured thickness using calipers was greater than the measured thickness using the laser profilometry system. Thus, the specimens with larger thickness gradients, which were statically calculated using the range in the histogram of thickness measured across one disk, usually resulted in higher volume differences compared to thickness measurements using calipers. This trend is highlighted in Figure 10. Differences as large as 5% were noted between the two volumetric calculation methods.

Therefore, for the disks analyzed here, it is recommended that thickness variations measured using the laser profilometry system be considered directly in pre- and postirradiation calculation of disk volumes. In addition, for future disk scans, the discrete delay data acquisition methodology will be applied to minimize edge artifacts associated with the technique.

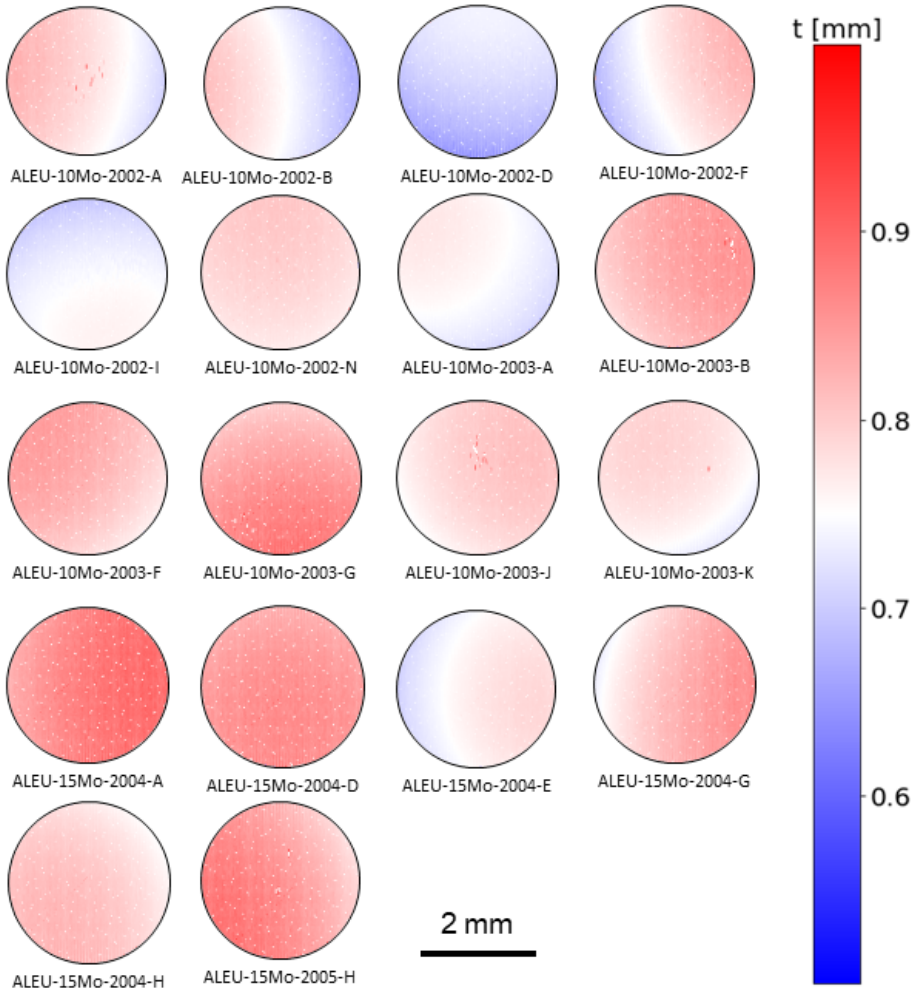

Figure 9. Thickness maps of 18 analyzed U–Mo MiniFuel specimens, showing significant specimen-to-specimen variation.

Table 1. Volume estimations using caliper, profilometry, and hybrid methods

Sample Name	Disk Radius [mm]		Disk Thickness [mm]		Volume [mm^3]				Difference [%] (Caliper vs. Keyence Methods)		
	Caliper (R_c)	Keyence (R_k)	Caliper (t_c)	Keyence (t_k)	V_k (Convex Hull)	R_k + t_k	R_c + t_k	R_c + t_c	V_k (Convex Hull)	R_k + t_k	R_c + t_k
10Mo-2002-A	1.50	1.40	0.800	0.786	4.97	4.84	5.52	5.62	11.55%	13.84%	1.75%
10Mo-2002-B	1.47	1.40	0.767	0.746	4.66	4.59	5.03	5.17	9.95%	11.19%	2.74%
10Mo-2002-D	1.48	1.40	0.729	0.692	4.37	4.26	4.76	5.02	12.94%	15.06%	5.08%
10Mo-2002-F	1.49	1.41	0.801	0.763	4.89	4.78	5.32	5.59	12.45%	14.41%	4.74%
10Mo-2002-I	1.49	1.41	0.755	0.732	4.70	4.59	5.07	5.23	10.19%	12.28%	3.05%
10Mo-2002-N	1.48	1.40	0.807	0.799	5.09	4.92	5.46	5.52	7.70%	10.80%	0.99%
10Mo-2003-A	1.50	1.42	0.751	0.747	4.90	4.76	5.28	5.31	7.68%	10.25%	0.53%
10Mo-2003-B	1.50	1.42	0.866	0.856	5.48	5.46	6.01	6.08	9.89%	10.21%	1.15%
10Mo-2003-F	1.50	1.41	0.852	0.840	5.46	5.26	5.94	6.02	9.30%	12.59%	1.41%
10Mo-2003-G	1.49	1.41	0.876	0.879	5.62	5.51	6.13	6.11	7.96%	9.83%	0.34%
10Mo-2003-J	1.50	1.43	0.811	0.804	5.29	5.13	5.68	5.73	7.76%	10.52%	0.86%
10Mo-2003-K	1.51	1.44	0.793	0.781	5.19	5.07	5.56	5.64	8.01%	10.17%	1.51%
15Mo-2004-A	1.51	1.42	0.940	0.915	6.10	5.84	6.51	6.69	8.84%	12.74%	2.66%
15Mo-2004-D	1.52	1.44	0.896	0.886	6.01	5.75	6.39	6.46	7.02%	10.99%	1.12%
15Mo-2004-E	1.51	1.44	0.790	0.762	5.09	4.97	5.46	5.66	10.02%	12.24%	3.54%
15Mo-2004-G	1.51	1.44	0.836	0.832	5.51	5.40	5.92	5.95	7.34%	9.22%	0.48%
15Mo-2004-H	1.51	1.45	0.836	0.814	5.54	5.40	5.79	5.95	6.80%	9.17%	2.63%
15Mo-2005-H	1.51	1.44	0.896	0.880	5.88	5.71	6.30	6.42	8.44%	10.99%	1.79%

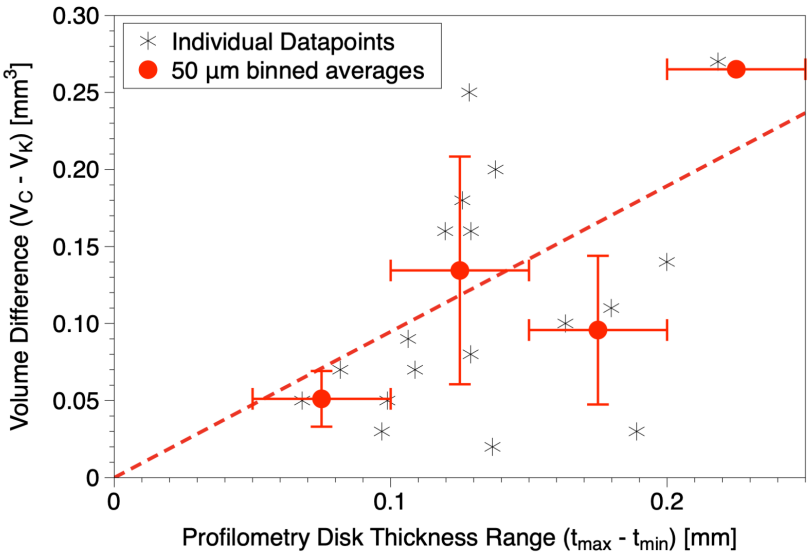

Figure 10. The difference in calculated disk volume as computed using caliper and Keyence thicknesses as a function of the range of thicknesses observed for each MiniFuel disk.

3. SERIAL SECTIONING WITH IN SITU DATA COLLECTION

3.1 SYSTEM SPECIFICATIONS

Serial sectioning has been used recently in a number of nuclear applications, including pore evolution and interface stitching in encapsulated nuclear fuel surrogates [5], high burnup structure in nuclear fuel [6], and high-resolution porosity characterization in graphite for nuclear applications [7]. The general basis of this form of serial sectioning is using combined focused ion beam (FIB) and scanning electron microscope (SEM) techniques together to gain information about a selected region in a material. Thus, it being called *FIB-SEM tomography*, or *serial sectioning*. The process involves alternating ion milling and SEM imaging to gain an image stack of 100+ images that are then reconstructed into a 3D form through image processing. This process allows scientists to observe a more targeted volume (on a lower magnification scale) than that obtainable through a traditional transmission electron microscopy sample by a factor of more than 100.

For this project, a ThermoFisher Scios DualBeam FIB/SEM is used to simultaneously mill and image material. A block is created by milling trenches out of the chosen bulk material using a 30 kV, 15 nA ion beam. The surface of interest is protected by a Pt cap deposited before any milling. The block edges are cleaned at lower beam currents until a cube or rectangular block is formed in the bulk. A fiducial mark, typically an *X* made using Pt, is created to keep the software aligned during the milling process. Then, ThermoFisher Auto Slice and View automated software is used to mill the surface of the material at a chosen depth and then image the freshly exposed surface. This process is continued through a chosen depth of the material, creating a stack of .tiff images. Because of limitations with instrument availability and the time-consuming nature of the data collection, the largest feasible dimensions that can be milled are typically blocks of 25 × 25 × 25 µm without using a plasma FIB. This is usually sufficient to cover grain boundaries or interfaces in material and sometimes large enough to examine multiple grains, depending on the target material.

For the purposes of this work, a U–Mo disk was used. A 12.5 × 12.5 × 12.5 µm targeted area was chosen, which is shown in Figure 11. A 0.5 nA beam was then used to mill 50 nm into the chosen surface, and images were collected for reconstruction. A total of 114 images were collected for this test run, which means that approximately 12.5 × 12.5 × 5.7 µm of material was probed.

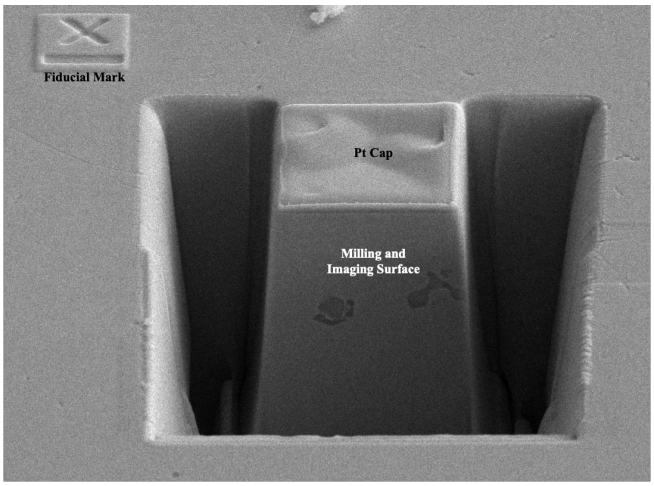

Figure 11: Example of a milled block ready for serial sectioning.

3.2 3D POROSITY RECONSTRUCTION

In its most basic form, the serial sectioning reconstruction process uses image segmentation technology to separate features, materials, and pores into labels, which can then be analyzed for quantitative and qualitative information. For this test case, ThermoFisher software Avizo 9.7.0 was used. Images were tilt corrected, aligned, sheared, and cropped before segmentation. Image segmentation used a combination of built-in contrast thresholding tools and manual adjustments. An example of the resulting segmentation is shown in Figure 12(a) and (b), where (b) shows an example of a 3D reconstruction of the pores within the U–Mo material.

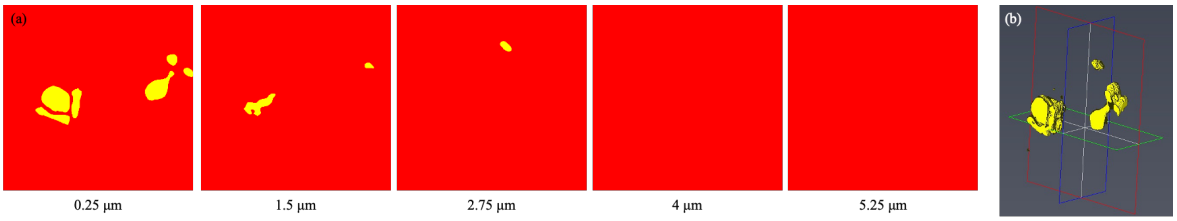

Figure 12. (a) Example of segmentation as a function of depth into the block. Red is U–Mo, yellow represents pores, and (b) is a 3D rendering of the pores.

From this segmentation, quantitative information about the pores in the material can be extracted, as well. In this sample, there are eight pores total in the material, ranging from 0.001 to 6.589 μm^3 in size, and the pores are listed in Table 2. There is a lower bound for detecting pores and precipitates, depending on the resolution of the scan. In general, pores smaller than 100 nm in diameter cannot be differentiated from background/contrast. Although the locations of the pores in this test subject are irrelevant, it is possible to extract where the pores are located relative to the targeted block of material or features within it. By targeting specific locations like grains and interfaces or certain locations radially along a sample, this same methodology can be used to study precipitates or pores that may preferentially form along grain boundaries or to study the burnup structure of the irradiated MiniFuel LEU disks intended for future study. Additionally, pore shape can be determined from the breadth, thickness, and width maximums determined in the sample, which may be beneficial for certain applications like high-burnup structure analysis.

Table 2. Pore volume measurement from 3D reconstruction.

Pore	Volume (μm^3)
1	0.017
2	2.996
3	6.589
4	0.002
5	0.167
6	0.002
7	0.001
8	0.010

3.3 IN SITU ENERGY DISPERSIVE X-RAY SPECTROSCOPY AND ELECTRON BACKSCATTER DIFFRACTION

Recently, the ability to simultaneously collect energy dispersive x-ray spectroscopy (EDS) and electron backscatter diffraction (EBSD) during the serial sectioning process has become more available. The Scios FIB/SEM used in this study comes with this capability. An EDAX Octane Elite Super Silicon Drift Detector EDS detector and an EDAX Velocity EBSD camera are mounted on the FIB/SEM system in such an orientation that data can be collected while serial sectioning is occurring. This setup allows for EDS and/or EBSD spectra to be collected at chosen intervals through the bulk milling process—for example, after every ten slices of material are milled and imaged, the milling can pause and allow time for EDS/EBSD collection. Additionally, both signals can be collected simultaneously to save time using the built-in EDAX software.

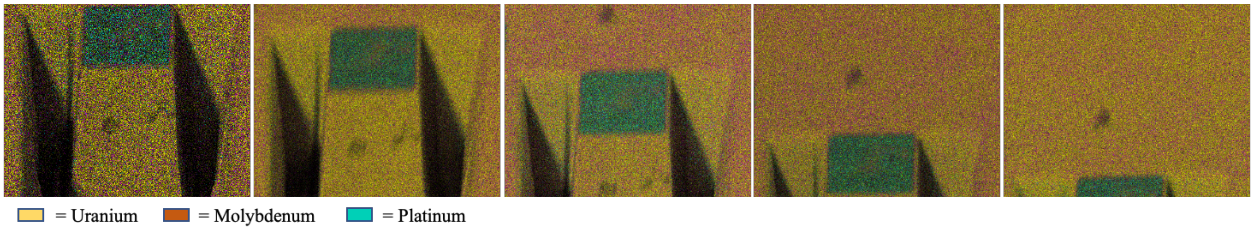

Figure 13: Example of the EDS that failed on the first attempt of the serial sectioning.

A test run of the software using EDS only was collected with the dataset in Figure 13. However, parameters were not as optimal as anticipated, and the software failed to collect results after the first few slices because of issues with the fiducial mark, as shown in Figure 13, in which drift from the inability to properly read the fiducial mark can be seen. A second test is ongoing. An additional test run is planned to include EBSD as well, once the EBSD detector returns from unanticipated system repairs.

4. CONCLUSIONS AND FUTURE WORK

This work highlights the new capabilities at ORNL with respect to laser profilometry and serial sectioning within the context of analyzing U–Mo MiniFuel disk specimens. The laser profilometry system provided more accurate results than those of the simple caliper measurements of MiniFuel disk thicknesses, and differences in volume calculations reached 5%. These differences, if not quantified initially, could otherwise have been falsely attributed to irradiation growth or swelling following High Flux Isotope Reactor irradiation for these specimens.

ORNL's nuclear fuel serial sectioning capabilities were also highlighted using the same U–Mo MiniFuel disk specimens. Even in the as-manufactured state, the U–Mo fuel volume analyzed using serial sectioning contained intrinsic porosity with a total volume of ~10 μm^3, which equates to approximately 1% internal porosity before irradiation. These types of analyses will prove invaluable when correlating the postirradiated MiniFuel microstructure to macroscale dimensional property measurements and will be applied to the optimized alpha-U disks eventually to be irradiated for the Mini-99 irradiation campaign.

5. REFERENCES

[1] National Research Council, *Medical Isotope Production without Highly Enriched Uranium*, National Academies Press, Washington, DC (2009). https://doi.org/10.17226/12569.
[2] I. N. Goldman, N. Ramamoorthy, P. Adelfang, "Fostering New Sources of Mo-99 for International Nuclear Medicine Needs: the Contribution of the IAEA Coordinated Research Project on Molybdenum-99 Production from LEU or Neutron Activation," Proceedings of the RETR International Meeting on Reduced Enrichment for Research and Test Reactors (2008).
[3] S. J. S. Dittrich, "History and Actual State of Non-HEU Fission-Based Mo-99 Production with Low-Performance Research Reactors," *Science and Technology of Nuclear Installations*, **2013** (2013).
[4] A. J. Kuperman, *Nuclear Terrorism and Global Security: The Challenge of Phasing out Highly Enriched Uranium*, Routledge Press, New York (2013).
[5] J. D. Arregui-Mena, R. L. Seibert, T. J. Gerczak, "Characterization of PyC/SiC Interfaces with FIB-SEM Tomography," *Journal of Nuclear Materials,* **545** 152736 (2021).
[6] C. McKinney, R. Seibert, G. Helmreich, A. Aitkaliyeva, K. Terrani, "Three-Dimensional Bubble Reconstruction in High Burnup UO_2," *Journal of Nuclear Materials*, **532** 152053 (2020).
[7] J. D. Arregui-Mena, P. D. Edmondson, A. A. Campbell, Y. Katoh, Site Specific, High-Resolution Characterisation of Porosity in Graphite Using FIB-SEM Tomography, *Journal of Nuclear Materials*, **511** (2018).